Journal of Volcanology and Geothermal Research 184 (2009) 333–346

Contents lists available at ScienceDirect

Journal of Volcanology and Geothermal Research

journal homepage: www.elsevier.com/locate/jvolgeores

Long-term variation of the shallow tremor sources at Aso Volcano from 1999 to 2003

Noriaki Takagi [a], Satoshi Kaneshima [a,*], Takahiro Ohkura [b], Mare Yamamoto [c], Hitoshi Kawakatsu [d]

[a] Dept. of Earth and Planet. Sci., Univ. of Kysuhu, Japan
[b] Aso Volcanological Obs., Univ. of Kyoto, Japan
[c] Dept. of Earth and Planet. Sci., Univ. of Tohoku, Japan
[d] Earthquake Research Institute, Univ. of Tokyo, Japan

ARTICLE INFO

Article history:
Received 29 July 2008
Accepted 20 April 2009
Available online 6 May 2009

Keywords:
continuous volcanic tremor
seismic array observations
source location
frequency domain analyses
long-term variation
phreatic eruption
shallow volcano edifice

ABSTRACT

In order to investigate the continuous volcanic tremor of Aso Volcano in Japan, we performed a series of temporary short-period seismic array observations near the Nakadake first crater (the active crater) during five years from 1999 to 2003. We deployed in all of the temporary observations a seismic array at the same location about 700 m west of the active crater, in order to investigate long-term changes in the tremor activity. In 1999 and 2003, another array was simultaneously deployed at a different location 700 m north of the crater to help locate the tremor sources. We developed a frequency domain semblance method and applied it to the waveform data of the frequency range where the continuous tremor is dominant (3–6 Hz). We measured arrival azimuths and slownesses of the continuous tremor signals as functions of frequency, which are then used to locate the epicenters of the tremor signals corresponding to the principal peaks of the power spectra.

For the observations in 1999 and 2002, the continuous tremor amplitudes are relatively small, and the slowness of the tremor signal observed at the west array takes a local minimum (0.5 to 0.6 s/km) near the frequency (~4.7 Hz for 1999 and ~4.8 Hz for 2002) which corresponds to the highest spectral peak. This implies that body waves dominate the tremor signals at the west array around the frequency. The tremor epicenters corresponding to 4.7 Hz for the observation in 1999 are located at the west rim of the currently active crater. While the surface crater activity of Aso remains low and the tremor activity is not clearly linked with the surface activity until early 2003, a close link between the tremor and crater activity appears in the middle of 2003, when a small phreatic eruption occurred a month before the array observation (July 10, 2003). Tremor signals of the observation in 2003 show a large spectral peak (4.2 Hz) where the slowness measured for the west array is very large (1.1 s/km), clearly suggesting that surface waves are dominant. The epicenter is again located at the western rim of the active crater. We interpret these observations as follows: in 1999 and 2002 when the surface activities of Aso were low, the continuous tremor excitation was deep and inactive. In the middle of 2003 when Aso Volcano became active with a series of phreatic eruptions a shallower tremor source was activated, possibly masking the deeper sources. This shallowing of the dominant tremor source could be due to the increase in the volcanic gas flow rate triggered by the phreatic eruptions.

1. Introduction

1.1. Activity of volcanic tremor

Seismic events observed at active volcanos can be classified as volcano tectonic earthquakes or as non-tectonic events. In this study we focus on"volcanic tremor" or simply "tremor", one of the non-tectonic volcanic signals, whose characteristic is its continuous occurrence. Seismic waves of volcanic tremor sometimes show one or more sharp spectral peaks which are typically interpreted as the results of resonance of underground resonators such as conduits, fluid-filled cracks (Chouet, 1986), and bubble clouds ascending in the conduit (Chouet et al., 1997). Examples include the tremors of Soufriere Hills (Neuberg et al., 2000), Sakurajima (Maryanto et al., 2008), Kilauea (Almendros et al., 2001), Deception Island (Ibanez et al., 2000), Pavlof (Garces et al., 2000), and Satsuma-Iwojima (Ohminato, 2006). A different class of physical model to explain the generation of continuous tremor is offered by Julian (1994). According to his model, non-linear oscillation of flow inside a vertical crack connecting two reservoirs generates continuous signals whose spectral feature changes with time. Iwamura and Kaneshima (2005) propose a steam/water mixture flow model for the generation of long period continuous tremor.

Features of volcanic tremor at an active volcano often change with time, reflecting changes in surface activity. Falsaperla et al. (2002)

* Corresponding author.
E-mail address: kane@geo.kyushu-u.ac.jp (S. Kaneshima).

0377-0273/$ – see front matter © 2009 Elsevier B.V. All rights reserved.
doi:10.1016/j.jvolgeores.2009.04.013

observed at Etna that the amplitudes of LP events and tremor fluctuate with changes in the surface activity of the volcano, though they focus on the LP events without intensively investigating the tremor. Jousset et al. (2003) observed low-frequency volcanic earthquakes and tremor at the Soufriere Hills volcano in Montserrat. The time interval between two consecutive low-frequency earthquakes often decreases preceding a dome collapse or an explosion, when the individual low-frequency earthquakes eventually merge to form a continuous tremor. At the Sakurajima volcano, the types of earthquake and tremor change depending on the position of the magma ascending through the conduit. Although there are many observations of the changes in features of volcanic tremor concomitant with changes in other

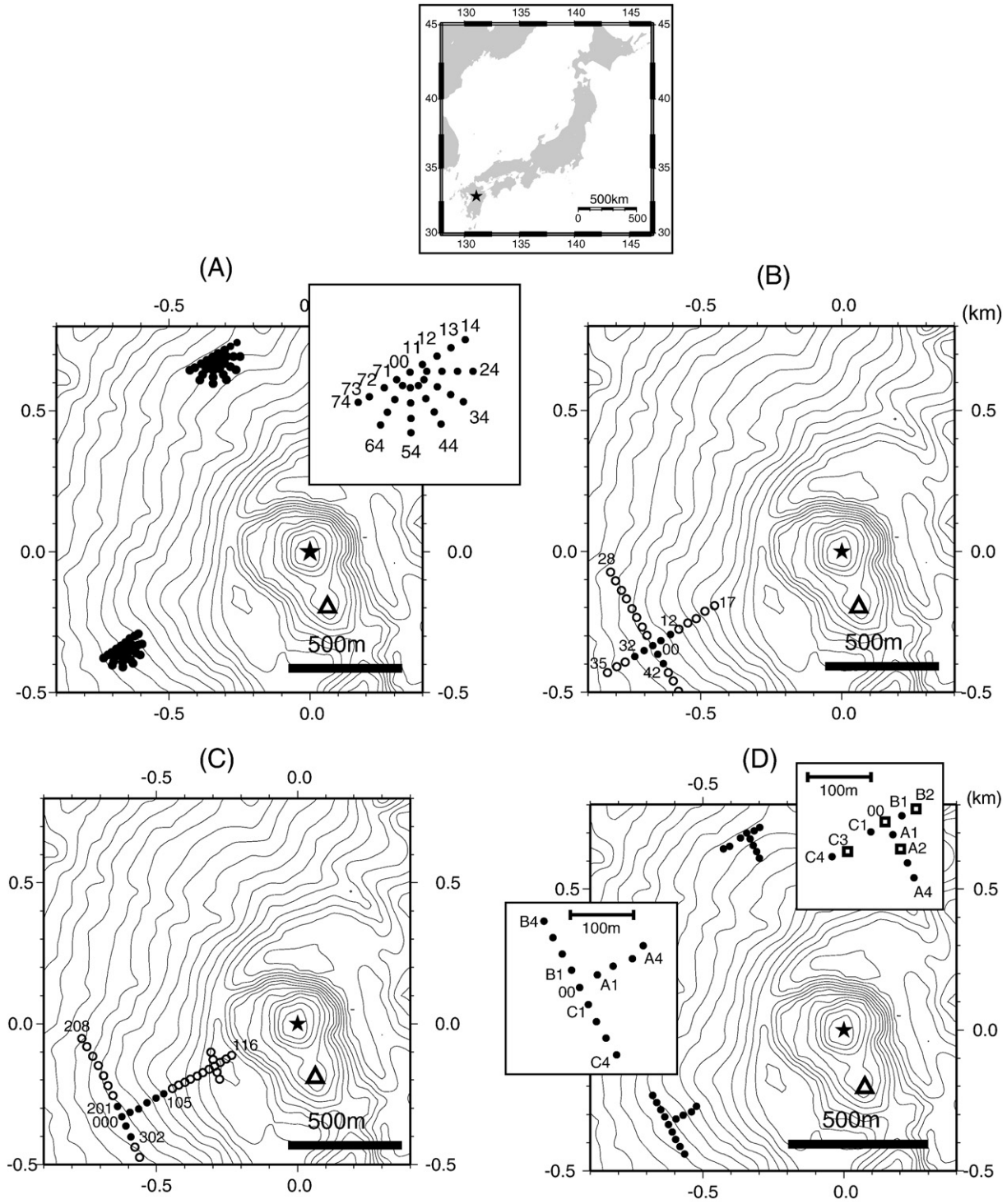

Fig. 1. Top: The location of Aso Volcano (star in the map). Bottom (A) to (D): Topography maps of the Nakadake (also called the active crater). One tick of the axes corresponds to 100 m. Topography contour interval is 10 m. Star marks the center of the active crater. Triangle shows the location of an older crater which has been inactive since major eruptions in the mid 1930's. (A): Solid dots show the locations of the sensors of the two arrays deployed approximately west (the W99 array) and north (the N99 array) of the active crater during the 1999 observation. Enlarged figure of the arrays is also shown to indicate the sensor numbers. (B) and (C): The locations of the arrays for the 2001 (W01) and the 2002 (W02) observations. Solid and open dots show the locations of sensors which are used and unused for the analyses of this paper, respectively. Selected sensors are labeled. (D): The locations of the arrays deployed during the 2003 observation (W03 and N03). Enlarged figures of the arrays are also shown. For the north arrays, dots and open squares are the sensors used for the N03 array in the first stage, and open squares are the sensors used for the N03 array in the second stage.

Table 1
Details of the array observations.

Array name	Date	Vertical sensor	Logger type	3-comp. sensor locations	Sampling dynamic range
W99	1999 Nov. 24–26	†	HAKUSAN	†	100 Hz
N99			LS-8000SH		16 bits
W01	2001 July 20–22	L22D	HAKUSAN	none	100 Hz
		2 Hz	LS-8000SH		16 bits
W02	2002 Nov. 8–10	L22D	HAKUSAN	000 106 113 208	200 Hz
		2 Hz	LS-8000SH	308 402 502	16 bits
W03	2003 Aug. 07–11	L22D	HAKUSAN	00	200 Hz
N03		2 Hz	LS-7000XT		16 bits
	Aug. 27–28		LS-8000SH		

The internal clocks of the data loggers were corrected with GPS signals once every hour. The locations of the sensors were determined by the GPS quick static location technique. (†) See Takagi et al. (2006).

volcanic activities, few studies investigate long-term variations of tremor activity, encompassing both quiet and active stages. Furthermore, few studies investigate changes in the location of tremor sources concomitant with changes in other volcanic activities with high accuracy, except for the study of the 1986 eruption of Izu-Oshima Miharayama using short period array processing (Furumoto et al., 1990) and those for Mt. Etna using tremor amplitude distribution (Carbone et al., 2008) and by continuous short period seismic array monitoring (Di Lieto et al., 2007). We note here that one of the main reasons for this lack of data is the difficulty in determining the location of volcanic tremor.

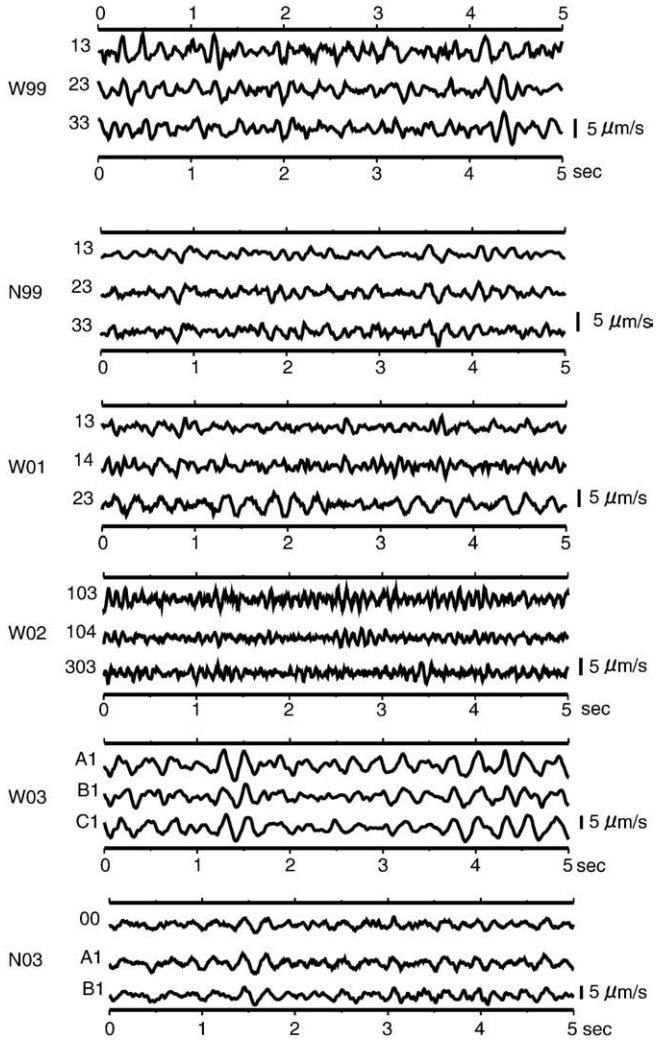

Fig. 2. Examples of the vertical component seismograms of three sensors of each array for 5 s. From top to bottom: W99, N99, W01, W02, W03, and N03. The numbers left of each trace indicate the sensor numbers (see Fig. 1 for the locations of the sensors).

1.2. Tremor location using dense seismic arrays

Processing short period seismic array data is the most powerful tool to locate tremor sources. Several studies have investigated volcanic tremor using one or more dense seismic arrays. For Etna two source regions are located for volcanic tremor by two arrays which are deployed at different azimuths from the crater but give inconsistent results (Saccorotti et al., 2004). The inconsistency is attributed to path effects such as bending of the rays due to complex velocity structure of the volcano edifice (Saccorotti et al., 2004). Almendros et al. (2001) deployed three seismic arrays around the Halemaumau pit crater at Kilauea. They resolve three different clusters of the LP event sources and a source of continuous tremor by applying the MUSIC method to the array data. In this study, we investigate the source locations of the continuous tremor at Aso, using short period array observations and data analyses, with special interest in the long-term changes of the tremor features and their relationship to the surface crater activity.

1.3. Volcanic tremors at Aso Volcano

Aso Volcano consists of several central cones and a caldera. There are 7 craters at the Nakadake summit (Fig. 1), one of the central cones currently and historically active. One of the craters (solid star in Fig. 1) is currently active and emits volcanic gases continuously. In this study we will call this crater either the Nakadake first crater or as the active crater. Recently Takagi et al. (2006) classified volcanic tremors at Aso into 3 types: (1) long period event-like tremor with a period of about 15 s; (2) isolated event-like tremor with dominant frequency around 1 to 2 Hz; and (3) tremor with dominant frequency around 3 to 10 Hz, which occurs continuously. We call type (3) tremor "continuous tremor" or simply "tremor". The source of the long period events (type 1) is located about 400 m south-west of the active crater at depths of 1 to 1.5 km (Kaneshima et al., 1996; Legrand et al., 2000; Kawakatsu et al., 2000). The source mechanism of the events is a combination of isotropic expansion/contraction and inflation/deflation of an inclined tensile crack (Kaneshima et al., 1996; Yamamoto et al., 1999; Legrand et al., 2000). On the other hand, the sources of the isolated events (type 2) are located south-east of the active crater, at a depth of about 600 m (Yamamoto, 2004). Yamamoto (2004) also reports that the source mechanism of the isolated events mainly consists of a radial motion of the sidewall of a nearly vertical cylinder. Takagi et al. (2006) analyse seismic array data and determine the location of the source of continuous tremor in 1999 and 2001, but they do not attempt to

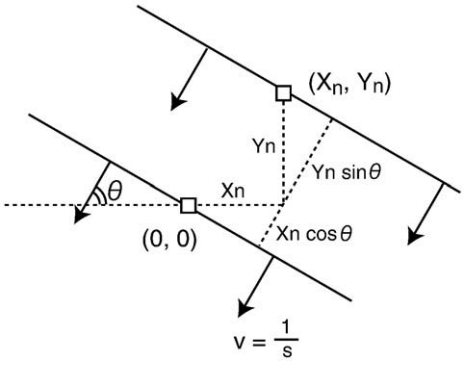

Fig. 3. Schematic figure for calculating time lags with respect to the array center using Eq. (1). (0, 0) and (X_n, Y_n) stand for the array center and the n-th sensor, respectively. Biases in azimuth caused by the plane wave approximation are less than 4° (Takagi et al., 2006) and insensitive to frequency.

Table 2
The averaged slownesses for the west-arrays.

Array name	Peak frequency (frequency band) Hz	Averaged slowness (s/km)
W99	4.7 (4.49 to 4.89)	0.67
W01	3.9 (3.61 to 4.00)	0.94
	4.6 (4.49 to 4.69)	0.91
W02	4.8 (4.69 to 4.98)	0.52
W03: Aug. 07–11	3.6 (3.52 to 3.81)	0.53
	4.2 (4.10 to 4.39)	1.02
W03: Aug. 27–28	3.6 (3.52 to 3.81)	0.43
	4.2 (4.10 to 4.39)	1.10

investigate the frequency dependence of the tremor features. In this study we analyze the short period seismic array data for a longer span of time, including those used by Takagi et al. (2006). We present the results from extensive investigations of the frequency dependence of the tremor signals. We shall also discuss the long-term variation of tremor signals during the time including the phreatic eruptions in 2003.

2. Array analyses

2.1. Array observations

We deployed short period seismometer arrays near the active crater of Aso Volcano four times in five years from 1999 to 2003 in order to observe volcanic tremors. Fig. 1 shows the location of each array and the locations of the sensors. Details of the observations are listed in Table 1. Examples of the observed seismograms are shown in Fig. 2.

2.2. Method: frequency domain semblance

In this study seismic signals arriving at the arrays are regarded as plane waves. We determine, by array processing of the observed seismograms, two parameters which represent the characteristics of a plane wave arriving at each array, θ and s, which stand for the arrival azimuth of the wave at the array measured counterclockwise from east, and the apparent slowness (in s/km) of the wave, respectively (Fig. 3). We call these parameters "wave parameters" in this study. We assume that all sensors are on the same horizontal plane, and do not determine the hypocentral depth directly. The bias caused by this assumption is discussed in Takagi et al. (2006). The velocity structure is assumed to be homogeneous for the array processing, but we shall consider horizontally layered velocity structure later when we investigate the wave type and the source depth of the continuous tremor.

Semblance (Neidell and Taner, 1971) is often used for seismic array analyses to quantify signal coherency. Since semblance is defined as the ratio of coherent signal power to the total power, one of its advantages is that it is not seriously biased by large fluctuations in wave energy. Large isolated events are frequent at Aso and show markedly different features from the continuous tremor we detect. Since we wish to use the longest possible time series to accurately determine the wave parameters of the continuous tremor, semblance is an ideal choice. We also wish to investigate the frequency-dependent properties of tremor signals, since they could play key roles in understanding the mechanism of continuous tremor. Since semblance cannot readily be applied to frequency analyses because, in its original form, it was defined in the time domain, in this study we newly develop a method of "frequency domain semblance".

Consider the case in which a plane wave arrives at a seismometer array. The time series of signal at the n-th sensor of the array is indicated as $u_n(t)$, while the time lag of the plane wave for the n-th sensor with respect to the array center (τ_n) (Fig. 3) is written as

$$\tau_n = -s(X_n \cos\theta + Y_n \sin\theta) \quad (1)$$

Here s stands for the slowness of the plane wave. X_n and Y_n are the (east and north) Cartesian coordinates of the n-th sensor relative to the center of the array, and θ is the back azimuth of the incident plane wave measured counterclockwise from east. The total number of sensor for the array is N.

Following Lacoss et al. (1969), we define the "beam" of the seismograms as,

$$b(\theta, s, t) = \frac{1}{N}\sum_{n=1}^{N} u_n(t + \tau_n(\theta, s)) \quad (2)$$

Stacking seismograms over the sensors is done in the time domain, unlike the f-k spectrum method (Lacoss et al., 1969) in which stacking is done in the frequency domain. This allows the extension of our method to the use of any wave front shape other than that of a plane wave, but at the cost of stacking efficiency. We denote the power spectrum density of b of the j-th time window as $R_j(\theta, s, f)$, where f means frequency. Guided by the original definition of the time domain semblance coefficient which has a physical meaning as the ratio of

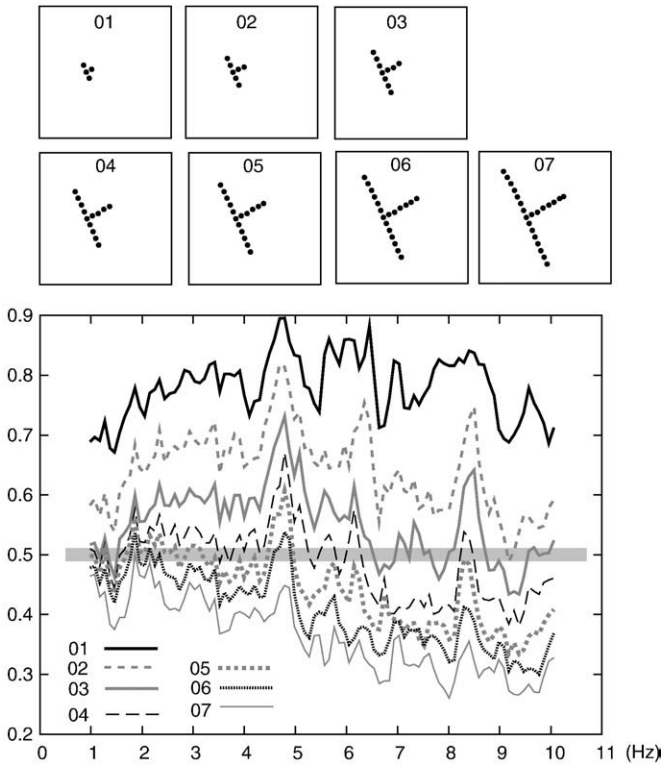

Fig. 4. The semblance values calculated for the arrays reduced from the W02 array. The numbers attached to the lines indicate the numbers of the sensors in each of the three segments of the whole W02 array around the array center (000, see also Fig. 1C) which are retained to form each reduced array (see top panels for the geometry of the reduced arrays). For instance, 03 means there are 10 stations retained in the reduced array. Horizontal axis shows frequency, and the vertical axis shows the semblance values.

Table 3
The averaged slownesses for the north-arrays.

Array name	Peak frequency (frequency band) Hz	Averaged slowness (s/km)
N99	4.7 (4.49 to 4.98)	0.61
N03: Aug. 07–11	3.6 (3.52 to 3.81)	0.62
	4.2 (4.10 to 4.39)	0.64
N03: Aug. 27–28	3.6 (3.52 to 3.81)	0.60
	4.2 (4.10 to 4.39)	0.59

coherent signal power to the total power (Neidell and Taner, 1971), we newly define the"frequency domain semblance" S as follows:

$$S_j(\theta, s, f) = R_j(\theta, s, f) / P_j(f). \quad (3)$$

where $P_j(f)$ stands for the averaged power spectral density for the j-th window. We denote the power spectrum density u_n ($n = 1, 2, \ldots N$) of the j-th time window as $P_j^n(f)$, and $P_j(f)$ is defined as the average of $P_j^n(f)$ over the N sensors.

In this study, we use two types of the data window with different lengths, "short window" and "long window". The length of a short window is 10.24 s, and each of the short windows does not overlap with the adjacent ones. The length of a long window is 400 s, and each of the long windows does not overlap with the adjacent ones. Equation

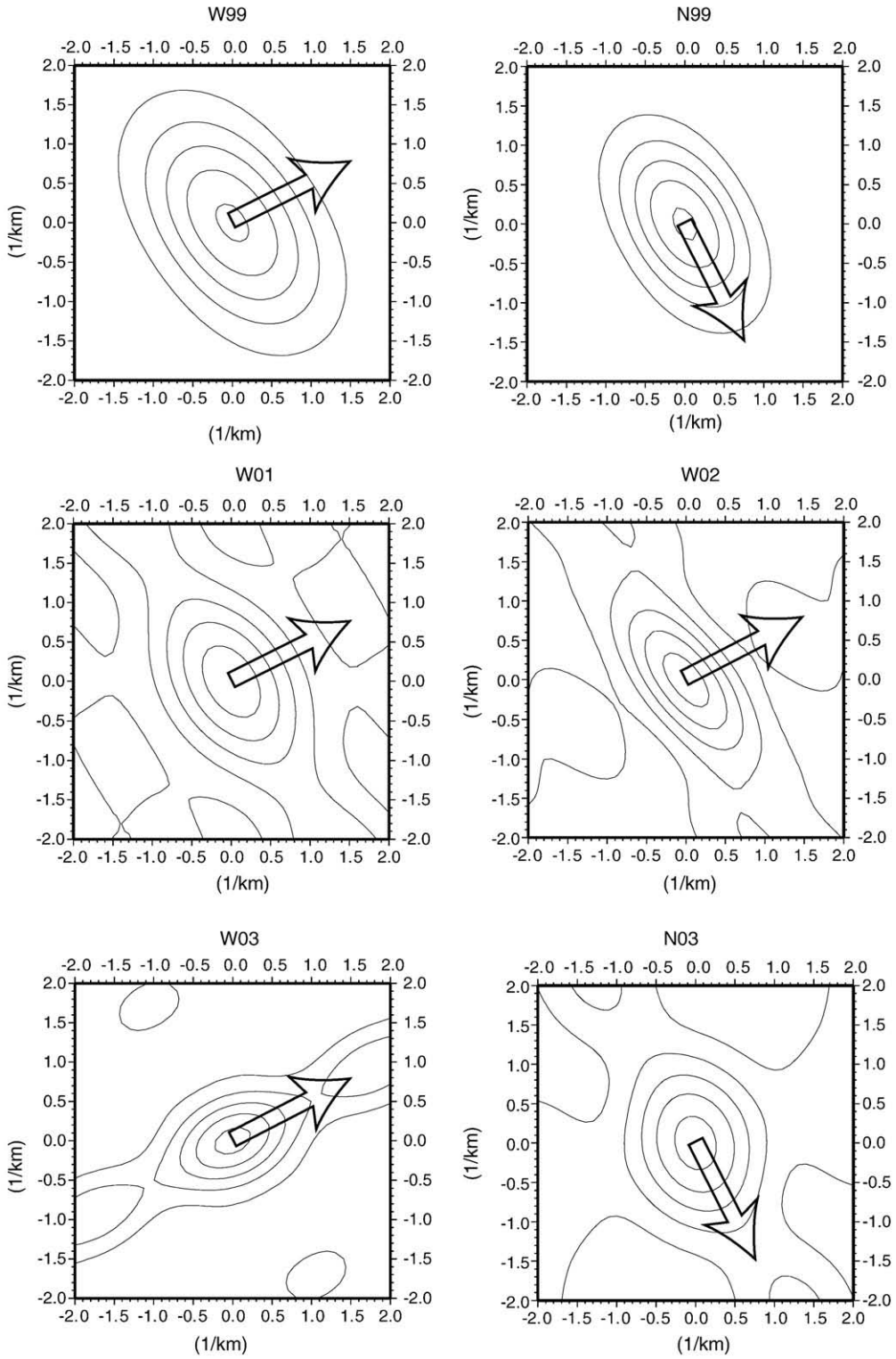

Fig. 5. The window functions calculated for each array. Open arrows indicate the azimuth to the center of the active crater (Nakadake, star in Fig. 1). The horizontal and vertical axes indicate wavenumber in 1/km. Tremor signals mostly arrive from the crater, so that for the west arrays (W99, W01, W02, and W03) the slowness resolution is good, while the azimuth resolution is poor, and vice versa for the north arrays (N99 and N03).

(3) states that S_j is the proportion of the power of a beam or coherent signal relative to the total power in the j-th time window for the frequency f, which is consistent with the original physical meaning of semblance (Neidell and Taner, 1971). The semblance coefficients $S_j(\theta, s, f)$ are calculated for each short window. After we calculate $S_j(\theta, s, f)$, we average them over several frequencies around the target frequency and over the short time windows contained in the l-th long window to obtain $\bar{S}_l(\theta, s)$. The parameter set $(\hat{\theta}_l, \hat{s}_l)$ for which $\bar{S}_l$ takes the maximum value is regarded as the most probable estimate of the parameter set for the l-th long window. We finally obtain the best estimates of the wave parameters by averaging $(\hat{\theta}_l, \hat{s}_l)$ for all of the long windows (Tables 2 and 3). We also adopt the standard deviations for both parameters as their uncertainty ranges (Figs. 7–10).

Here we check the consistency of our frequency domain semblance method with the original time domain semblance method (Neidell and Taner, 1971) using the observed seismograms of 400 s starting from 22:00:00 on November 26, 1999. We also compare the results from our method with that by the f-k spectrum method (Lacoss et al., 1969). For the frequency domain semblance method, we use short-windows of 10.24 s, and long-windows of 400 s. For the f-k spectrum method, we use a window of 10.24 s, and the estimated wave parameters are averaged over 400 s. For the time domain semblance method, we apply nine different narrow band-pass filters to the seismograms, with the center frequencies separated by 1 Hz (1.7, 2.7,..., 8.7, and 9.7 Hz) and with the band width of 0.5 Hz. The length of the time window is 0.5 s, and we obtain 800 band-passed seismograms for each of the nine band-pass filters, to which the time domain semblance method is applied to determine the wave parameters. We average the 800 sets of the wave parameters for each of the nine pass bands. For the frequency range from 3 to 6 Hz, the results from the comparisons between the wave parameters obtained by the three different methods show good agreement with each other, with differences in slowness and azimuth of about 0.05 s/km and 5° at most for the frequency range we consider (3 to 6 Hz). The use of frequency domain semblance developed in this study is therefore justified.

2.3. Selecting waveform data for array analyses

The observed signals in general are more complicated at the receivers nearer to the active crater of Aso, and the coherency can be very low even between two seismograms which are recorded at two places separated only by a few hundred meters. We check the relation between the array size and the overall waveform coherency among the west arrays. The aperture of the W02 array which has the largest number of sensors (37) in our study is reduced to several different lengths by retaining only a certain number of sensors around the array center (sensor 000, Fig. 1C), and the averaged semblance values are estimated for each reduced aperture length as a function of frequency. Fig. 4 shows the averaged semblance values calculated for several reduced arrays for the W02 array. The aperture length of a reduced array is represented by the number of retained receivers from the array center (000) in three directions, ranging from 01 (retaining 4 stations) to 07 (22 stations). It is shown clearly that the larger the array aperture, the smaller is the signal coherency. When the coherency between the seismograms is too low, say below 0.5 (corresponding to 05 to 07 in Fig. 4), we should expect seismic array processing methods to not yield good results. Guided by this result we reduce the aperture lengths of the W01 and the W02 arrays to nearly 200 m (see Fig. 1B and C for the sensor locations of the reduced arrays). These are close to the aperture length of W99, which facilitates the investigation of the long-term variations of the wave parameters. Fig. 5 shows the spectral window functions defined in Lacoss et al. (1969) for the W99, N99, W03, and N03A arrays, and the reduced arrays of W01 and W02. Hereafter we call the reduced arrays of W01 and W02 as the W01 and W02 arrays, for simplicity.

Fig. 6 shows the averaged power spectra of the four observations. The spectra are averaged over time and sensors used for the array analyses. In this study we focus on the spectral peaks between 3 Hz and 6 Hz to investigate the wave parameters. This is because the isolated event-like tremors (type 2) are dominant for frequencies lower than 3 Hz (Takagi et al., 2006), and because for frequencies higher than 6 Hz surface waves with much lower coherency over the arrays are dominant and lack prominent spectral peaks in the spectra of the 2001 and 2003 observations.

Within the frequency range between 3 Hz and 6 Hz, we choose for determining the wave parameters narrower frequency bands where power spectral peaks exist. For the 1999 and 2003 data, we choose the peaks which are shared by both of the north and west arrays. For the 2001 and 2002 data, we choose all of the dominant peaks in the range between 3 Hz and 6 Hz. Tables 2 and 3 show the center frequencies and frequency bands used in the array analyses which are measured for the arrays deployed on the western flank of the active crater (W99, W01, W02, and W03), and on the northern flank of the crater (N99 and N03), respectively. The band widths approximately correspond to the half widths of the spectral peaks.

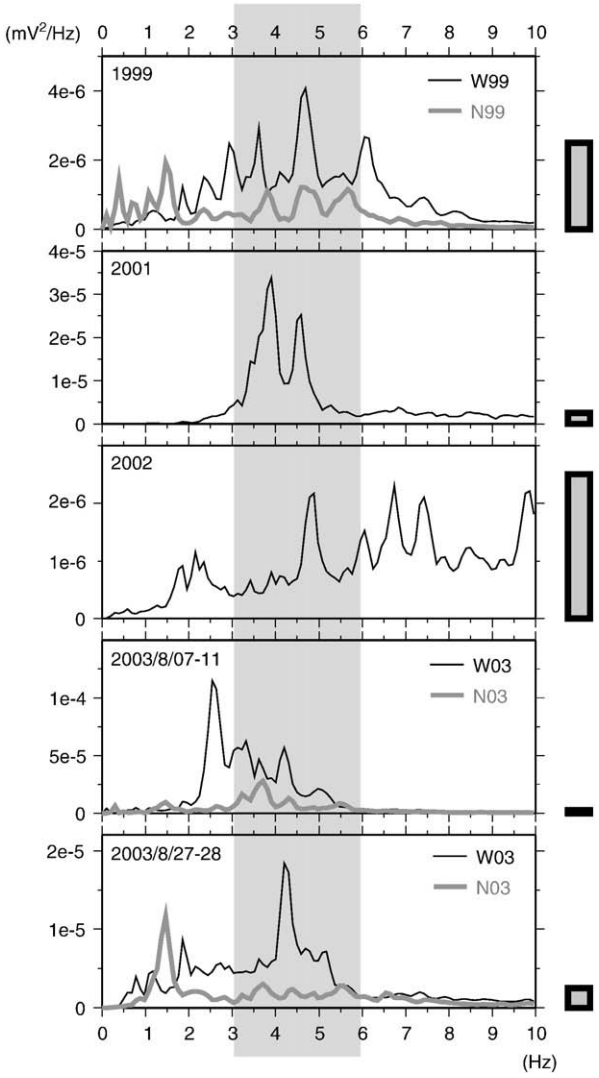

Fig. 6. Averaged power spectra for each observation (from top to bottom: 1999, 2001, 2002, 2003 first stage, and 2003 second stage). For the observations in 1999 (top panel) and 2003 (bottom two panels), dark line and light gray line show the spectra of the arrays deployed at the western and northern flank of the active crater, respectively. The frequency range used for array analyses in this study (from 3 to 6 Hz) is shown by shade. The gray bars at the vertical axes at the right side indicate the power of 2×10^{-6} (μV^2/Hz). 1×10^{-6} mV^2/Hz corresponds to 0.0013566 $(\mu m/s)^2$/Hz.

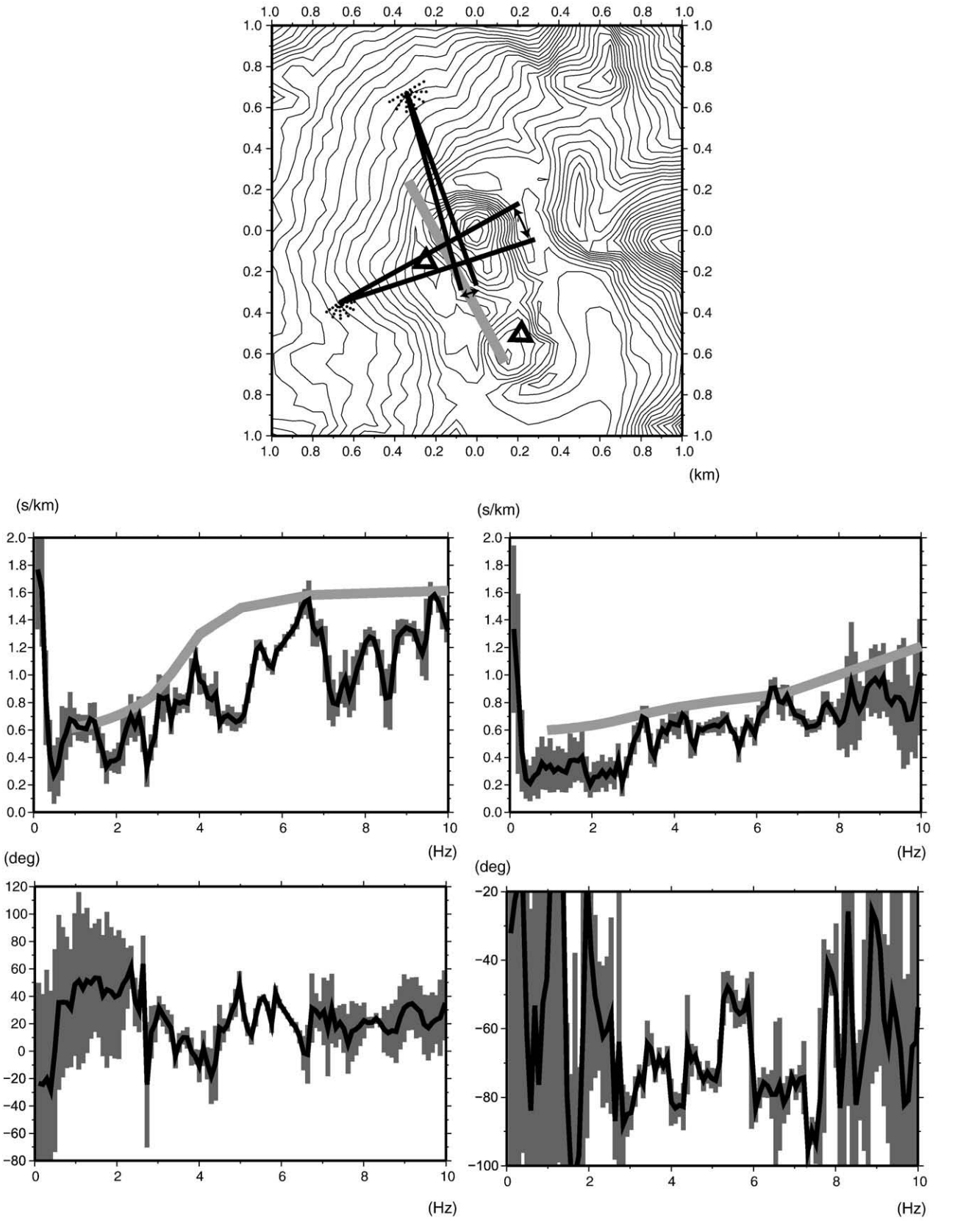

Fig. 7. Top: Arrival azimuths of the tremor signals around 4.7 Hz for the 1999 observation plotted on a topography map. Dots represent the sensors of the W99 and N99 arrays. The solid black lines (and the acute angle between the two lines) show the estimated range (67%) of the arrival azimuths measured for each array. The area surrounded by the four solid lines is regarded as the epicentral region. The thick gray line represents the surface projection of the upper limit of the crack-like conduit (Yamamoto et al., 1999). Triangles show the locations of the two tremor sources determined by Takagi et al. (2006). Middle: slowness averaged over the entire observation period as a function of frequency for the W99 array (middle left) and the N99 array (middle right), with error bars representing one sigma (standard deviation). Smooth gray curves in the middle two panels indicate the Rayleigh wave dispersion curves. See text and Table 4 for the velocity structures for W99 and N99. Bottom: Signal azimuth averaged over the entire observation period as a function of frequency for the W99 array (bottom left) and the N99 array (bottom right). The azimuths to the center of the active crater are 30° and −65° for the W99 and N99 arrays, respectively.

3. Results of the analyses

3.1. Summary of the results

The averaged spectra of the 1999 observation period is shown at the top panel of Fig. 6. The dark and gray solid lines represent the averaged power spectra of the W99 and N99 arrays, respectively. For the focused frequency range (3 to 6 Hz), the two spectra share only one peak at 4.7 Hz, although they both have three spectral peaks in the frequency range. This would imply that the peaks except for the one at 4.7 Hz are formed by site and/or path effects. We therefore focus on the spectral peak at 4.7 Hz hereafter for the estimation of the wave

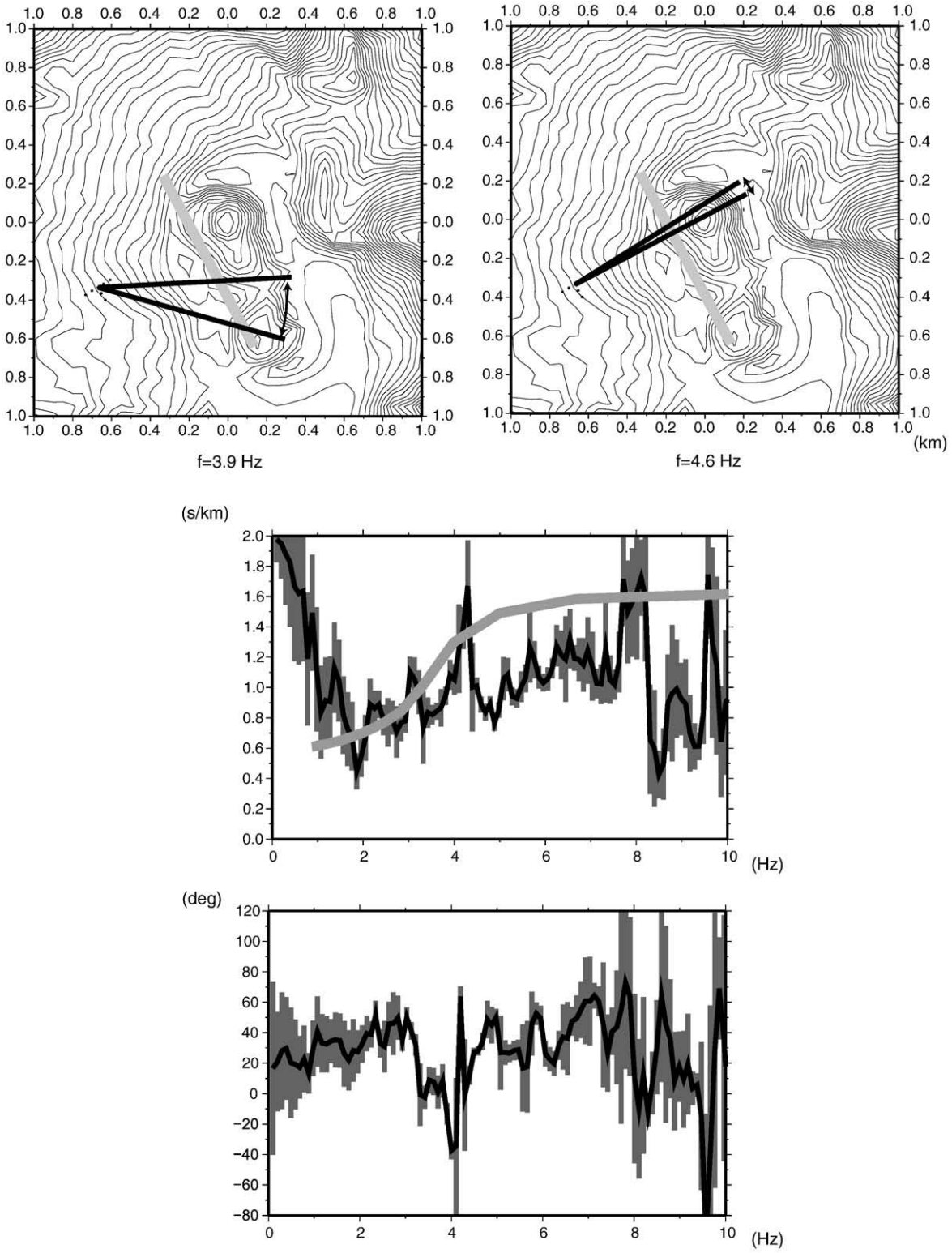

Fig. 8. Top: Arrival azimuths of the tremor signals around 3.9 Hz (left) and around 4.6 Hz (right) for the 2001 observation (W01). Middle: Slowness averaged over the entire observation period as a function of frequency for W01. Gray curve in the middle panel indicates the Rayleigh wave dispersion curve for the velocity model for the W99 array (Table 4). Bottom: Signal azimuth. Other details are the same as Fig. 7.

parameters. The signals arrive broadly from the direction of the active crater for most of the frequencies higher than 3 Hz (Figs. 7–10).

Fig. 7 shows the estimated arrival azimuths of the continuous tremor for the W99 and N99 arrays at 4.7 Hz, projected on a topography map around the active crater. The solid lines represent the azimuthal ranges estimated for the two arrays using all data. The azimuth estimated for each long window should be regarded as the center of the epicentral distribution for each long (400 s) window, and we call it the "long window epicenter". For 67% of the long windows the estimated azimuths fall inside these ranges. Hence the area surrounded by the four solid lines can be regarded as the distribution of the long window epicenters. The area extends approximately north to south between the crack-like conduit (gray line west of the crater in the map (Yamamoto et al., 1999)) and the active crater, with its southern edge reaching a crater which has been inactive since major eruptions in the mid 1930's (Fig. 1). Fig. 7 also shows the estimated slownesses as a function of frequency for the W99 (middle left) and the N99 (middle, right) arrays. For the W99 array, the slowness takes a local minimum near 4.7 Hz (Table 2) which is the frequency of the highest peak of the power spectrum (Fig. 6). This indicates that body waves (S and/or P) are dominant in the signals corresponding to the peak for the W99 array. For the N99 array, on the other hand, the frequency (4.7 Hz) does not clearly corresponds to a local minimum of the slowness (Table 3), so that we cannot readily judge what types of waves dominate the tremor signals of the N99 array from this alone.

The spectral power of the W01 array in 2001 is about 10 times larger than that for the W99 array, and two overwhelmingly dominant peaks are seen at the frequencies of 3.9 and 4.6 Hz (second row of Fig. 6). Since only one array (W01) was deployed at the western flank in this observation (Fig. 1), we adopt both peaks to estimate the wave parameters. Fig. 8 shows the estimated azimuths projected on a topography map (top) and the averaged slowness for each frequency (middle). The slowness for the frequency of 4.6 Hz (Table 2) is significantly larger than that of the corresponding spectral peak at 4.7 Hz observed for the W99 array. A local minimum of the slowness does not clearly exist around 4.7 Hz, unlike that of the W99 array (Fig. 8).

For the 2002 observation period (W02), a large spectral peak is observed at 4.8 Hz in the frequency range from 3 to 6 Hz (third row of Fig. 6). Fig. 9 shows the estimated azimuths for 4.8 Hz on a map (top), and the measured slowness as a function of frequency (middle). The averaged slowness at 4.8 Hz (Table 2) corresponds to a local minimum of the slowness, as in the case of the W99 array. These observations suggest that body waves are dominant in the tremor signal corresponding to the spectral peak at 4.8 Hz.

The fourth and bottom rows of Fig. 6 show the averaged spectra of the observations during the first (August 7 to 11) and the second (August 27 to 28) stages of the 2003 observation, respectively. During this observation period, the tremor amplitudes are much larger than the observations in 1999 and 2002. We shall focus on two spectrum peaks at around 3.6 Hz and 4.2 Hz, which are shared by the two arrays, W03 and N03. Fig. 10 shows the estimated azimuths plotted on a topography map. In the first stage (August 7 to 11), the estimated azimuth from the W03 array for the weaker peak at 3.6 Hz is quite unstable, so that we cannot determine the epicenter region (Fig. 10, top left, thin lines). The slowness for W03 (Table 2) is markedly smaller than that observed at the W99 array and indicates that body waves are dominant. On the other hand the azimuth for the stronger spectral peak (4.2 Hz) is much more stable and the epicentral region corresponding to this peak for the first stage is located at the west rim of the active crater, above the upper rim of the crack-like conduit (Fig. 10, top left, thick lines). As we shall argue later, the high slowness of W03 (Table 2) indicates that body waves cannot be dominant in the tremor signals corresponding to this spectral peak. The features of tremor signals (Tables 2 and 3) and the epicenters (Fig. 10, top and third row right) for the second stage of the 2003 observation are similar to the first stage.

3.2. Long-term variations of the apparent slowness

One of the noble aspects of the data set obtained from a series of temporary observations we performed for several years near the active crater of Aso is that it enables us to investigate the long-term variations of the characteristics of the continuous tremor sources, because the west arrays (W99, W01, W02, and W03) were deployed at the same site and we were able to adjust the array sizes to facilitate direct comparisons between the observations done at different times. Here we focus on the tremor signals corresponding to the spectral

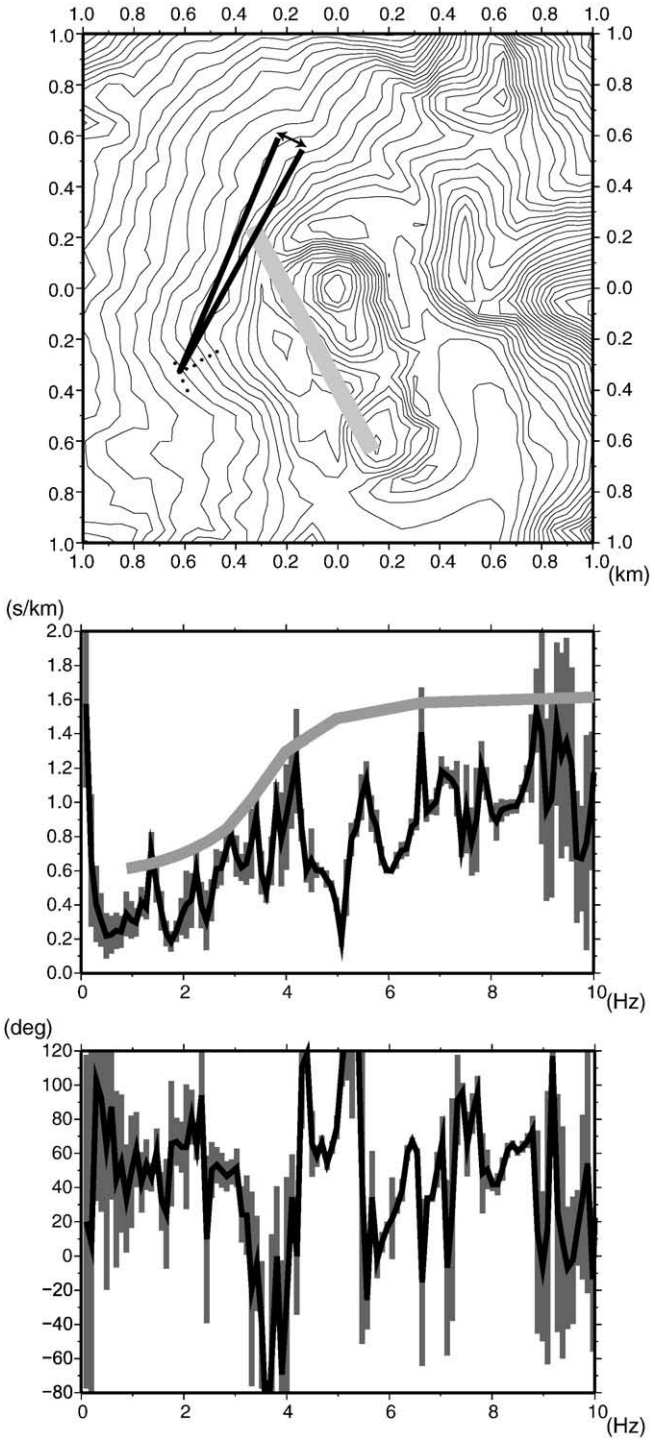

Fig. 9. Top: arrival azimuths of the tremor signals around 4.8 Hz (right) for the 2002 observation (W02). Middle: slowness averaged over the entire observation period as a function of frequency for W02. Bottom: signal azimuth. Other details are the same as Fig. 7.

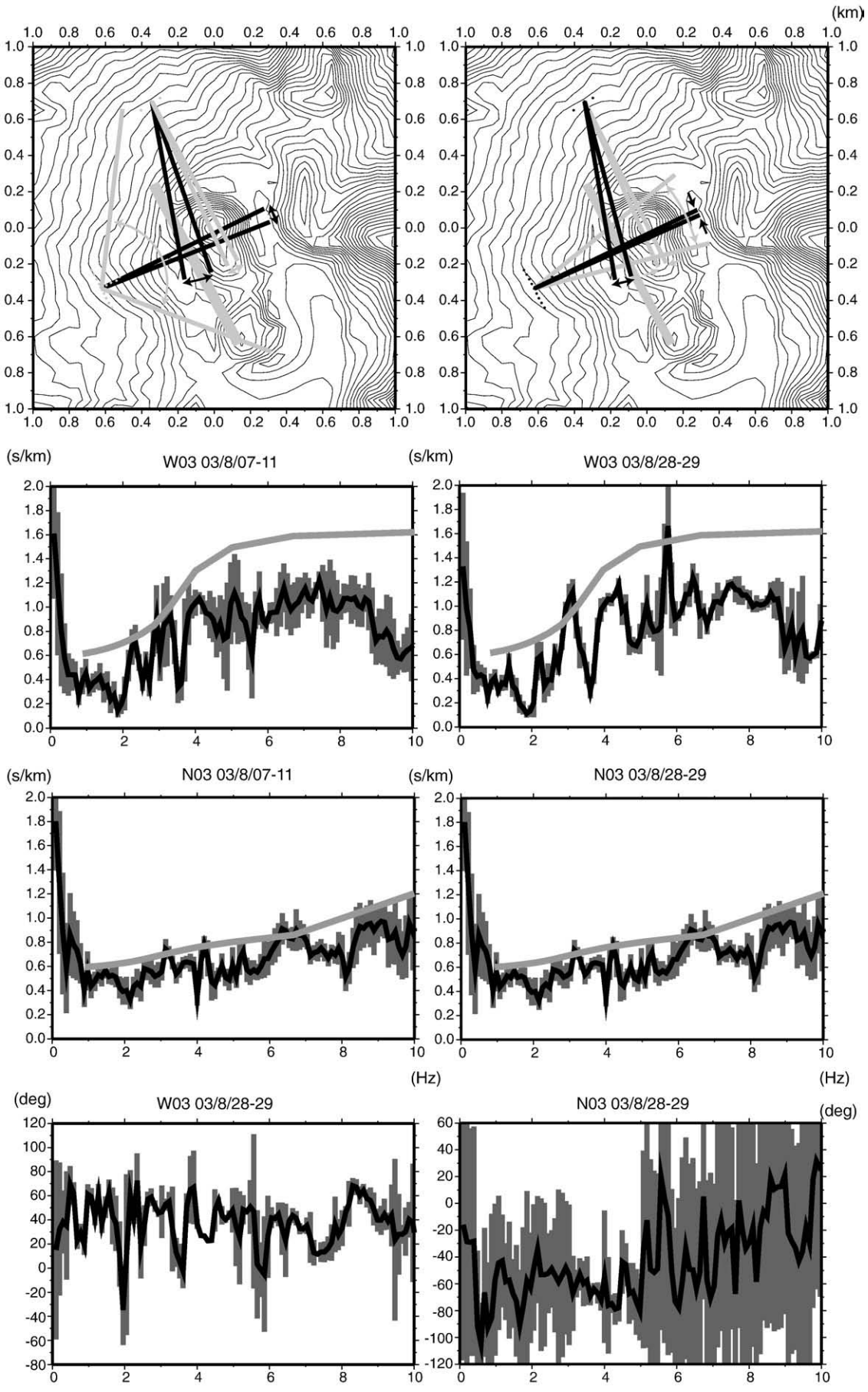
(km)
(s/km)
W03 03/8/07-11
(s/km)
W03 03/8/28-29
(s/km)
N03 03/8/07-11
(s/km)
N03 03/8/28-29
(Hz)
(Hz)
(deg)
W03 03/8/28-29
N03 03/8/28-29
(deg)

Table 4
The velocity models used to compute the dispersion curve, for W99 (top) and N99 (bottom), which have two layers above a homogeneous half space.

Dept range (m)	*Vp* (km/s)	*r* (g/cm^3)
0–80	1.2	1.8
80–200	2.7	2.2
200–	3.4	2.4
0–30	1.2	1.8
30–200	2.7	2.2
200–	3.4	2.4

The ratio *Vp*/*Vs* is fixed to be 1.8 throughout the layers and the half space.

peaks in the frequency range from 4 to 5 Hz. Each spectrum in Fig. 6 has only one large peak in this frequency band, and those peak frequencies remain approximately the same for the 1999, 2001 and 2002 observations. The estimated slownesses for the focused peaks at the western sites are listed in Table 2. During the 2001 and 2003 observations when the tremor amplitudes at the west arrays are large, the estimated slownesses are also large. As shown in the next section, this means that surface waves dominate the continuous tremor signals when the tremor amplitudes are large.

For the north arrays, the situation is not as good as with the west arrays, since the arrays were deployed only in 1999 and 2003. Nevertheless we still can make inferences on the long-term variations of the tremor signatures. The estimated slownesses for the N99 and N03 arrays remain remarkably stable (Table 3), regardless of a significant difference in the surface activity of the crater, as well as in the amplitude level and overall spectral features of the continuous tremor. Such stable slownesses are in marked contrast to those of the west arrays. This observation suggests that the type of the dominant waves at the north arrays remain the same.

3.3. Wave type of the tremor signals

For the W99 and W02 arrays located at the western flank of Nakadake (Fig. 1), the slowness takes a local minimum around the frequency of the largest spectral peak. On the other hand, for the W01 and W03 arrays the correspondence between the spectral peak and the slowness local minimum cannot be seen clearly. The high slowness suggests the dominance of surface waves over body waves. We check this hypothesis by investigating surface wave dispersion expected from the velocity structure of shallow edifice of Aso Volcano, although it is rather poorly known at this stage and should be highly complex. Tsutsui et al. (2003) propose a model of the P-wave velocity structure near the crater of Aso. In their model for the western flank of the crater, the P-wave velocities are 1.2 km/s, 3.4 km/s, and 3.8 km/s, at the surface, at 500 m depth, and at 1800 m depth, respectively. We start from their model to interpret the observations of the continuous tremor with assumptions about the *Vp*/*Vs* ratios and density. Several velocity and density structure models are constructed based on the model by Tsutsui et al. (2003) and are tested against the data by a process of trial and error. Dispersion curves of Rayleigh waves for flat layered half space are computed by using DISPER80 (Saito, 1988).

We consider that the vertical component of the waveform of the continuous tremor consists of body waves (P and S waves) and Rayleigh waves, and that the relative amplitude of each wave varies from frequency to frequency. We then regard the upper envelope of a complex slowness curve which is obtained by the frequency-domain semblance method as representing the Rayleigh wave dispersion. In the middle left panel of Fig. 7, the smooth gray line shows the dispersion curve calculated for the velocity model shown in Table 4 which fits the upper envelope of the estimated slownesses for the W99 array well. The troughs of the observed slowness curve with small slowness should correspond to the frequencies where the relative contributions of body waves are large.

In the middle right panel of Fig. 7, the calculated dispersion curve for the N99 array is superimposed on the observed slowness curve. Following Tsutsui et al. (2003), the velocity structure beneath the north arrays has a thinner surface layer than that beneath W99 (Table 4). As stated in the previous sections, the slowness of the peak frequencies for the north arrays are stable regardless of the large differences in the crater activity and tremor amplitudes, quite unlike those of the west arrays. The power spectra of the north arrays do not show marked local minima at the frequencies corresponding to the spectral peaks. We argue that the most reasonable explanation of these observations is that the tremor signals corresponding to the dominant spectral peaks of the north arrays mostly consist of Rayleigh waves. This is in marked difference from those of the west arrays for which the relative contributions between body waves and surface waves substantially change with time and with the crater activity.

Fig. 11 shows examples of the particle motions observed at the center of the W99, W02, and W03 arrays. A narrow band pass filter whose corner frequencies are 4.5 Hz and 5 Hz is applied to the observed three component seismograms in order to draw the diagrams. Although it is not clear what the wave type of the continuous tremor signals is, we can at least state that the vertical component is relatively large. In the case of the west arrays, below which there is a soft surface layer with P wave velocity of 1.2 km/s, the incident angles of P waves must be larger than 60°(from vertical downward) to explain a slowness value about 0.7 s/km as is observed for W99 (Table 2). A P wave with a large incident angle, in other words arriving nearly horizontally, cannot cause large vertical motions. We can therefore argue that the observed signals at the west arrays are not dominated by P waves, with possible exceptions of W02 array, whose relatively small vertical motions and small slowness (0.52 s/km for 4.8 Hz) might indicate a larger proportion of P waves. For the W99 array, we have shown that the tremor signals corresponding to the frequencies near 4.7 Hz are dominated by body waves, so that the body waves should consist mostly of S waves. On the other hand, the tremor signals of the W03 array are dominated by surface waves. In the case of the north arrays, we cannot discriminate the wave type of the signal from the particle motions, though they could be consistent with our proposition that Rayleigh waves are a significant part of the ground motion.

3.4. Source depth of the continuous tremor

We estimate the source depth of the continuous tremor observed at the W99 array based on the slowness of the tremor signals at the frequencies where S waves are dominant (near 4.7 Hz) using ray tracing for the 1-D velocity structures. Two velocity models are used, both of which are modified from the *Vp* model proposed by Tsutsui et al. (2003) assuming a constant *Vp*/*Vs* ratio (1.8). The first model has velocity jumps and is used for the analysis of the Rayleigh wave dispersion (Table 4, Fig. 7). The second model, on the other hand, has velocities that vary gradually with depth (*Vp* = 1.2 km/s at 80 m, *Vp* = 2.7 km/s at 200 m, *Vp* = 3.4 km/s at 500 m, respectively). For the W99 array, the averaged slowness for the signal around the main spectral peak at 4.7 Hz is 0.67 s/km (Table 2) with the uncertainty

Fig. 10. Top: Arrival azimuths of the tremor signals for the first (left: August 7 to 11) and the second stages (right: August 27 and 28) of the 2003 observation. The azimuths for the frequencies 3.6 Hz and 4.2 Hz are shown with light and dark lines, respectively. 2nd and 3rd rows: Slowness averaged over the entire observation periods of the first (left) and the second (right) stages as a function of frequency for the W03 array (2nd row) and the N03 arrays (3rd row). Gray curves indicate the Rayleigh wave dispersion curves for the velocity models for the W99 (2nd row) and N99 (3rd row) arrays, respectively (Table 4). Bottom: Signal azimuth for the second stage, for W03 (left) and N03 (right). Other details are the same as Fig. 7.

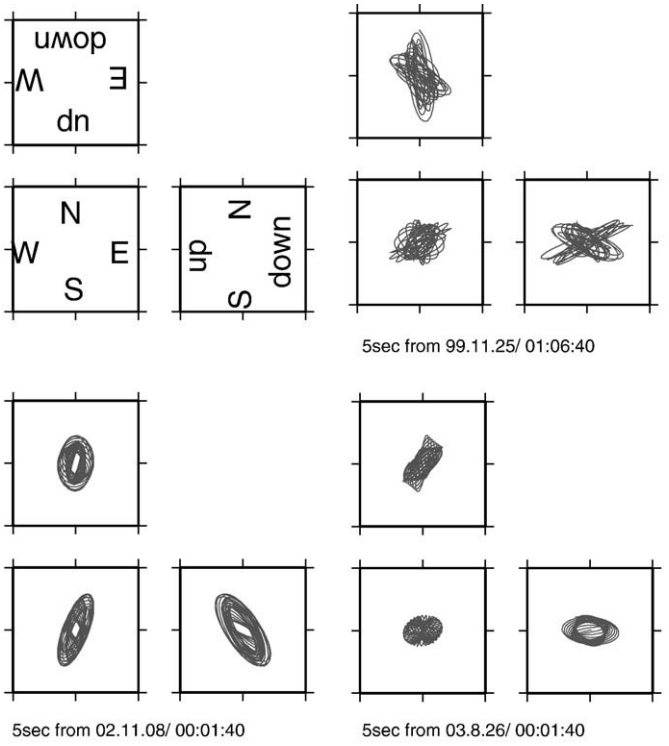

Fig. 11. Typical narrow band particle motions for a 5 s time window of the west arrays, for the W99 array (top right: 4.7 Hz), the W02 array (bottom left, 4.8 Hz), and the W03 array (bottom right, 4.2 Hz). In each example, panels at top, bottom right, and bottom left show narrow band particle motions projected to the E–W vertical section, to the N–S vertical section, and to the horizontal plane, respectively.

range between 0.62 s/km and 0.72 s/km. The distance between the W99 array and the estimated epicenter location is nearly 630 m. We use the two models mentioned above and assume for simplicity that the tremor signals are dominated by S waves. The estimated source depth is around 150 m below the crater lake for the gradual model (the second model), and about 300 m for the model with velocity jumps (the first model). The slope of the surface at the W99 array is ~10°. If the seismic velocity changes perpendicularly to the surface, the slope leads to the source depths nearly 100 m shallower than the estimates described above. For the N99 array, we cannot find an appropriate depth which explains the averaged slowness of 0.61 (s/km) because of a too fast P-wave velocity (3.4 km/s) of the layer near the surface beneath the N99 array. This supports the idea that Rayleigh waves are dominant at the northern site. Based on these considerations we argue that the source of the continuous tremor is located at shallow depth beneath the active crater, probably shallower than 300 m below the crater lake.

4. Discussion

4.1. Estimated locations of the tremor epicenters

The epicenters of the continuous tremor are reasonably well constrained for the data of the 1999 and 2003 observations in which the west and north arrays were operated simultaneously. For these observations we have determined the tremor epicenters for the signals corresponding to the peaks of power spectra which are shared by the two arrays (4.7 Hz for 1999 and 3.6 Hz and 4.2 Hz for 2003). Except for the 3.6 Hz peak of the 2003 observation, the epicentral regions of the continuous tremor are located around the west rim of the active crater and above the upper rim of the crack-like conduit detected by Yamamoto et al. (1999). We also have determined the source depths of the tremor signal corresponding to one of the spectral peaks of W99 (4.7 Hz) to be between 150 and 300 m below the crater lake, which is above the upper rim of the crack-like conduit (400 m below the lake). The excitation of the continuous tremor therefore seems related to the shallowest conduit system beneath the active crater of Aso. The heterogeneous velocity structure around the active crater may affect the tremor epicenter location, but quantitative evaluations of such effects are difficult given poor knowledge of the velocity structure. According to the results from numerical simulations performed for Kilauea by Almendros et al. (2001), the bias in signal azimuth due to heterogeneous structure and topography is nearly 10° for an array at the epicentral distance of 2.3 km. Since our arrays are located within a kilometer from the tremor epicenter, the effects of heterogeneous structure and topography would be less than 5° corresponding to the bias in the epicenter of about 100 m.

For the 2001 and 2002 observations, we could not determine the epicenters corresponding to the dominant spectral peaks by the frequency domain analyses developed in this study. Takagi et al. (2006) apply the conventional time domain semblance method which determines the source distance as well as the slowness and azimuth to the same data set as this study but by using the entire W99, N99 and W01 arrays and a much wider frequency band (2 to 10 Hz). They conclude that for the 1999 observation two sources exist outside of the apparent distribution of the apparent epicenters (two triangles in Fig. 7). For the 2001 observations, on the other hand, only one source is required and is located near the triangle in Fig. 7 located northwest of the crater lake. The same method as that of Takagi et al. (2006) is applied also to the data of the entire W02 array, giving an epicentral region approximately the same place as that of the W01 array. These

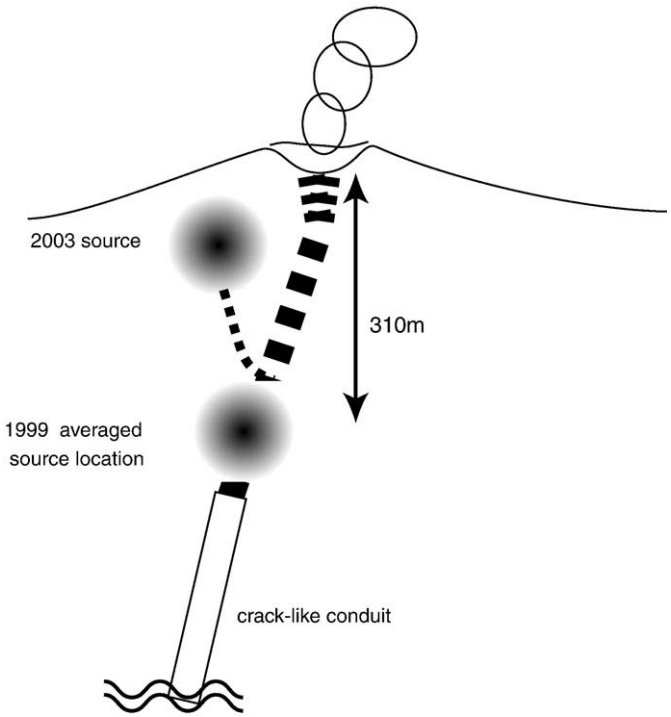

Fig. 12. Schematic figure of the arrangement of the conduits beneath the Nakadake viewed approximately from south. The upper edge of the crack-like conduit is about 400 m below the crater lake (Yamamoto et al., 1999). Shaded circle labeled "1999 averaged source location" indicates the averaged location of the hypocenter of the dominant continuous tremor around 4.7 Hz in 1999 determined by the semblance-based analyses and ray tracing based on the assumption that dominant wave type at W99 is S wave (see text for the details). Shaded circle labeled "2003 source" indicates the hypocenter of the continuous tremor which was activated after the phreatic eruption on July 10, 2003. Its depth is not well constrained but inferred to be shallow based on the dominance of Rayleigh waves at W03. Thick broken line indicates the main conduit which connects the crack-like conduit to the crater, while thin broken line indicates the narrow conduit to the west of the active crater.

suggest that the epicenters of the tremor sources tend to be located near the western to northwestern rim of the active crater, between the crater and the upper rim of the crack-like conduit.

4.2. Change of the dominant tremor source accompanying the activation of Aso in 2003

The volcanic activity of Aso remained low for several years before 2003 without major eruptive phenomena at the Nakadake first crater. In 2003 Aso Volcano became relatively active. The temperature beneath the south wall of the active crater increased gradually, reaching 530 °C in May, 2003. The water temperature of the crater lake also increased, exceeded 70 °C in May, and reached 81 °C in September (Japan Meteorological Agency, 2003). On July 10, a phreatic eruption occurred at the active crater and spray of mud consisting of wet ash was blown out of the crater. The Japan Meteorological Agency (JMA) reported that other minor phreatic eruptions have occurred on 12 and 14 July, 2003. An involvement of minor amount of fresh glass in the ash ejected at the time of the phreatic eruption on July 10 has been suggested (Hoshizumi et al., 2003), which however is inconclusive due to possible contamination of magma at the times of previous eruptions. The depth where the glass formed is not well constrained either but appears to be shallower than 400 m below the crater lake (Hoshizumi et al., 2003). The permanent network of broadband seismometers around the crater does not show any long period tremor (type 1) above the noise level at the time of the eruption, quite unlike a series of phreatic eruptions of similar intensity in 1994 (Kaneshima et al., 1996). These observations suggest that there was not significant magma or gas flow along the crack-like conduit at the time of the phreatic eruption itself, though the involvement of minor amount of juvenile magma cannot be ruled out.

Though with no long period tremor (type 1) concomitant with the eruption, broadband seismograms do show a marked increase in the amplitudes of long period tremor and slight changes in its spectral features which immediately follow the July 10 eruption and continue at least a few months. The amplitudes of higher frequency continuous tremor which we focus in this study also gradually increase reaching the maximum at the end of July, with a much longer delay than that of the long period tremor, nearly 10 days after the July 10 eruption. The long period tremor (type 1) with the longest eigenperiod of 15 s is known to be radiated by the oscillation of a crack-like conduit filled with volcanic gas or gas/ash mixture (Yamamoto, 2004). It is also reported that the amount of the (SO_2) emission increased (Saito et al., 2006) after the eruption. These observations combined with our knowledge about the shallow conduit arrangement beneath Aso suggest an increase following the eruption in the flow rate of volcanic gas through the crack-like conduit from the deep magma chamber. Although the eruption itself is likely to have occurred above the crack-like conduit (with its top at 400 m below the crater lake) and is unlikely to cause any significant gas or magma flows along the conduit due to the absence of volcanic tremor of type 1 and the minor amount of fresh glass at most (Hoshizumi et al., 2003), its occurrence seems to have eventually induced substantial changes in the conditions in the crack-like conduit, probably promoting more intensive gas flow along it.

At the time we deployed the W03 and N03 arrays, the amplitudes of the continuous tremor had culminated at their highest levels. As shown previously for the W03 array, the slowness of the continuous tremor corresponding to the strongest spectral peak at 4.2 Hz is quite large, suggesting the dominance of surface waves. This is strikingly different from the tremor features at the times of low volcanic activity such as the 1999 and 2002 observations, when the tremor amplitudes are small and the tremor slownesses corresponding to the main spectral peaks are low, suggesting the dominance of body waves. The simplest interpretation of this difference in the dominant wave type of the tremor is that the dominant tremor source depth changes at an eruption. This does not necessarily mean that a tremor source actually migrates vertically. A more realistic explanation is that there are multiple tremor sources which are separated vertically and the relative excitations from the sources change, triggered by minor eruptive events. While determining the deeper source's depth based on ray tracing is possible (150 m to 300 m beneath the crater lake), the depth of the source activated in 2003 whose surface waves are dominant on the array seismograms is harder to determine. It is natural, however, to anticipate that the dominant source in 2003 is shallower than the source in 1999 (Fig. 12). The shallower tremor source may thus be selectively activated relative to the deeper ones after phreatic eruptions, probably triggered by an increase in the gas supply from depths. This simple scenario does not apply in the case of the 2001 observation, when the amplitudes of continuous tremor were quite large and the corresponding tremor slownesses were large, but there was no obvious surface activity at the crater. This seems to exemplify a complex relationship between the volcanic surface activity and the tremor features, but we argue that it is consistent with our inference that magma does not play a major role in exciting continuous tremor at Aso at least in relatively quiet stages of its activity. As is quantitatively justified in Fig. 7 (middle right, dispersion curve), at the north arrays surface waves always dominate tremor signals, so that the slowness is solely controlled by the velocity structure below the array and remains about the same (see middle right of Fig. 7 and third row of Fig. 10). The excitation of surface waves to the north array or the conversion from body waves to surface waves along the path to the north array should be very efficient.

The extension of the crack-like conduit to the surface meets the active crater (Yamamoto et al., 1999), yet the most prominent source of the continuous tremor at the time of phreatic eruptions in 2003 seems away from the straight continuation of the crack-like conduit to the crater lake (Fig. 12). We speculate that the continuous tremor is excited by the interaction between the volcanic gas and a low-temperature aquifer through a mechanism of "condensation oscillation" (e.g., Nariai and Aya, 1983). The existence of aquifers a few hundreds meters beneath the active crater at Aso is indicated by magneto-telluric surveys (Hase et al., 2005). During the quiet stage, the gas flow would intrude into the aquifer at about 300 m depth and might generate the continuous tremor there. During the active stage such as in 2003, the increased gas flow would dry up the aquifer at the depth, and the volcanic gas could intrude into the shallower aquifer.

Acknowledgments

We thank all who participated in the observations: Y. Sudo, S. Yoshikawa, T. Tsutsui, T. Hashimoto, M. Kato, T. Ohminato, G. Helffrich, and T. Mori. We could not complete this work without their help. G. Helffrich kindly checked the English language of this paper. Discussion with Y. Sudo was particularly helpful. The comments by two anonymous referees were useful.

References

Almendros, J., Chouet, B., Dawson, P., 2001. Spatial extent of a hydrothermal system at Kilauea Volcano, Hawaii,determined from array analysis of shallow long-period seismicity. J. Geopyhs. Res. 106, 13565–13580.

Carbone, D., Zuccarello, L., Saccorotti, G., 2008. Geophysical indications of magma uprising at Mt Etna during the December 2005 to January 2006 non-eruptive period. Geophys. Res. Let. L06305. doi:10.1029/2008GL033212.

Chouet, B., 1986. Dynamics of a fluid-driven crack in three dimensions by the finite difference method. J. Geophys. Res. 91, 13967–13992.

Chouet, B., Saccorotti, G., Martini, M., 1997. Source and path effects in the wave fields of tremor and explosions at Stromboli Volcano, Italy. J. Geophys. Res. 102, 15129–15150.

Di Lieto, B., Saccorotti, G., Zuccarello, L., La Rocca, M., Scarpa, R., 2007. Continuous tracking of volcanic tremor at Mount Etna, Italy, Geophys. J. Inter. 169, 699–705.

Falsaperla, S., Privitera, E., Chouet, B., Dawson, P., 2002. Analysis of long-period events recorded at Mount Etna (Italy) in 1992, and their relationship to eruptive activity. J. Volcanol. Geotherm. Res. 114, 419–440.

Furumoto, M., Kunitomo, T., Inoue, H., Yamada, I., Yamaoka, K., Ikami, A., Fukao, Y., 1990. Twin sources of volcanic tremor of Izu-Oshima volcano Japan. Geophys. Res. Let. 17, 25–27.

Garces, M.A., McNutt, S.R., Hansen, R.A., Eichelberger, J.C., 2000. Application of wave-theoretical seismoacoustic models to the interpretation of explosion and eruption tremor signals radiated by Pavlof Volcano, Alaska, J. Geophys. Res. 105, 3039–3058.

Hase, H., Hashimoto, T., Sakanaka, T., Kanda, W., Tanaka, Y., 2005. Hydrothermal system beneath Aso Volcano as inferred from self-potential mapping and resistivity structure. J. Volcanol. and Geotherm. Res. 143, 259–277.

Hoshizumi H., Saito, G., Uto, K., Watanabe, K., Ikenobe, S., 2003, Morphology, chemical compositions, and origin of volcanic glasses in July 10, 2003 ash of Nakadake, Aso Volcano (in Japanese), Report of Coordinating Committee for Prediction of Volcanic Eruption, 96.

Ibanez, J.M., Del Pezzo, E., Almendros, J., La Rocca, M., Alguacil, G., Ortiz, R., Garcia, A., 2000. Seismo volcanic signals at Deception Island volcano, Antarctica: wave field analysis and source modeling. J. Geopyhs. Res. 105, 13905–13931.

Iwamura, K., Kaneshima, S., 2005. Numerical simulation of the steam-water flow instability as a mechanism of volcanic tremor. Geophys. J. Int. 163, 833–851.

Jousset, P., Neuberg, J., Sturton, S., 2003. Modelling the time-dependent frequency content of low-frequency volcanic earthquakes. J. Volcanol. Geotherm. Res. 128, 201–223.

Julian, B.R., 1994. Volcanic tremor: nonlinear excitation by fluid flow. J. Geophys. Res. 99, 11,859–11,877.

Kaneshima, S., Kawakatsu, H., Matsubayashi, H., Sudo, Y., Tsutsui, T., Ohminato, T., Ito, H., Uhira, K., Yamasato, H., Oikawa, J., Takeo, M., Iidaka, T., 1996. Mechanism of phreatic eruptions at Aso Volcano inferred from near-field broadband seismic observations. Science 273, 642–645.

Kawakatsu, H., Kaneshima, S., Matsubayashi, H., Ohminato, T., Sudo, Y., Tsutsui, T., Uhira, K., Yamasato, H., Ito, H., Legrand, D., 2000. Aso94: Aso seismic observation with broadband instruments. J. Volcanol. Geotherm. Res. 101, 129–154.

Lacoss, R.T., Kelly, E.J., Toksoz, N.M., 1969. Estimation of seismic noise structure using arrays. Geophysics 34, 2138.

Legrand, D., Kaneshima, S., Kawakatsu, H., 2000. Moment tensor analysis of near-field broadband waveforms observed at Aso Volcano, Japan. J. Volcanol. Geotherm. Res. 101, 155–169.

Maryanto, S., Iguchi, M., Tameguri, T., 2008. Constraints on the source mechanism of harmonic tremors based on seismological, ground deformation, and visual observations at Sakurajima volcano, Japan. J. Volcanol. Geotherm. Res. 170, 198–217.

Nariai, H., Aya, I., 1983. Pressure oscillations in vent tubes induced by system condensation in pressure suppression containment. Proc. on Nuclear Reactor Thermal-hydraulics, II 1128–1134.

Neidell, N.S., Taner, M.T., 1971. Semblance and other coherency measures for multichannel data. Gyophysics 36, 483–497.

Neuberg, J., Luckett, R., Baptie, B., Olsen, K., 2000. Models of tremor and low-frequency earthquake swarms on Montserrat. J. Volcanol. and Geotherm. Res. 101, 83–104.

Ohminato, T., 2006. Characteristics and source modeling of broadband seismic signals associated with the hydrothermal system at Satsuma-Iwojima volcano, Japan. J. Volcanol. Geotherm. Res. 158, 467–490.

Saccorotti, G., Zuccarello, L., Del Pezzo, E., Ibanez, J., Gresta, S., 2004. Quantitative analysis of the tremor wavefield at Etna Volcano, Italy. J. Volcanol. Geotherm. Res. 136, 223–245.

Saito, M., 1988. DISPER80: a subroutine package for the calculation of seismic normal-mode solutions. In: Doornbos, D.J. (Ed.), Seismological Algorithms. InAcademic Press, pp. 293–319.

Saito, M., Matsuo, N., Matsushima, K., Shimizu, H., Fukui, R., Ohta, K., 2006, SiO2 emission from Mt. Aso (in Japanese), Report of Coordinating Committee for Prediction of Volcanic Eruption, 101.

Takagi, N., Kaneshima, S., Kawakatsu, H., Yamamoto, M., Sudo, Y., Okura, T., Yoshikawa, S., Mori, T., 2006. Apparent migration of tremor source synchronized with the change in the tremor amplitude observed at Aso Volcano, Japan. J. Volcanol. Geothermal Res. 154, 181–200.

Tsutsui, T., Sudo, Y., Mori, T., Kattsumata, K., Tanaka, S., Oikawa, J., Tomatsu, T., Matsuo, N., Matsushima, K., Miyamachi, H., Nishi, K., Fujiwara, Y., Hiramatsu, H., 2003. 3-D seismic velocity structure beneath the edifice of central cones of Aso Volcano. Bull. Volcanol. Soc. Japan (Kazan) 48 293–3–7.

Yamamoto, M., Kawakatsu, H., Kaneshima, S., Mori, T., Tsutsui, T., Sudo, Y., Morita, Y., 1999. Detection of a crack-like conduit beneath the active crater at Aso Volcano, Japan. Geophys. Res. Lett. 26, 3677–3680.

Yamamoto, M., 2004, Volcanic fluid system inferred from broadband seismic signals, Doctor thesis of Tokyo Univ.